

# Topologically protected midgap states in complex photonic lattices

H. Schomerus

*Department of Physics, Lancaster University, Lancaster, LA1 4YB, United Kingdom*

(Dated: January 7, 2013)

One of the principal goals in the design of photonic crystals is the engineering of band gaps and defect states. Drawing on the concepts of band-structure topology, I here describe the formation of exponentially localized, topologically protected midgap states in photonic systems with spatially distributed gain and loss. When gain and loss are suitably arranged these states maintain their topological protection and then acquire a selectively tunable amplification rate. This finds applications in the beam dynamics along a photonic lattice and in the lasing of quasi-one-dimensional photonic crystals.

Since the inception of the field [1, 2], the design of photonic crystals with band gaps and defect states has been facilitated by drawing analogies to condensed matter systems. A novel impetus for such endeavors is provided by the discovery of topological insulators and superconductors, systems which occur in distinct configurations that cannot be connected without closing a gap in the band structure and consequently display robust surface and interface states [3, 4]. Recent works have started to transfer concepts of band-structure topology to the photonic setting. Thus far, this has opened up avenues for unidirectional transport [5, 6], adiabatic pumping of light [7], and creation of photonic Landau levels [8, 9], as well as the creation of bound and edge states via dynamic modulation in the time domain [10, 11].

The practical utility of topological concepts in photonics will depend much on the robustness versus absorption and amplification. These processes do not have an electronic counterpart; they render the effective Hamiltonian non-hermitian, and break time-reversal symmetry—but in a different way than a magnetic field, whose presence or absence enters the topological characterization of electronic band structures [12, 13]. One may therefore wonder whether topological protection can survive the presence of gain and loss.

Remarkably, as shown here for a complex version of the Su-Schrieffer-Heeger (SSH) model [14], such robustness can be demonstrated for a photonic realization of topologically protected midgap states, localized at an interface in the interior of the system. Under the influence of spatially distributed gain and loss [15–17], these states not only maintain their topological characteristics but also acquire desirable properties that do not have an electronic analogue—the midgap states can be selectively amplified without affecting the extended states in the system.

The selective amplification of the midgap state can be utilized in beam manipulation and lasing. For instance, the considered model can be realized as the coupled-model theory of a photonic lattice with alternating lattice spacings. In a setup with passive and lossy components, the midgap state can be rendered lossless while all other states suffer identical losses. This provides a mech-

anism to induce the midgap state in the beam propagation through a photonic lattice; the beam can then be manipulated via adiabatic pumping of light. In an alternative realization that includes active components, the midgap state constitutes a selectively amplified mode in a quasi-one-dimensional photonic crystal laser.

*Complex Su-Schrieffer-Heeger model.*—The SSH model was originally introduced to describe fractionalized charges in polyacetylene; an exponentially localized midgap state then forms at a defect in the dimerization pattern [14]. I consider a version (the cSSH model, shown in Fig. 1) which applies to photonic lattices and crystals and incorporates distributed loss and gain [15–17]. The original SSH model consists of a tight-binding chain with alternating coupling constants  $t_a$  and  $t_b$  (for being specific let us assume  $t_a > t_b > 0$ ), and a defect in this sequence which supports the topologically protected midgap state (see Fig. 1). The fundamental unit cell is composed of two sites (labeled A and B) with amplitudes  $\psi_n^{(A)}$  and  $\psi_n^{(B)}$ , where the integer  $n$  enumerates the unit cells. To explore the effects of loss and gain in photonic realizations I consider a staggered complex onsite potential  $i\gamma_A = i\bar{\gamma} + i\gamma$  on the A sites and  $i\gamma_B = i\bar{\gamma} - i\gamma$  on the B sites. This modification defines the cSSH model. The tight-binding equations read

$$\varepsilon\psi_n^{(A)} = i\gamma_A\psi_n^{(A)} + t'_n\psi_{n-1}^{(B)} + t_n\psi_n^{(B)}, \quad (1a)$$

$$\varepsilon\psi_n^{(B)} = i\gamma_B\psi_n^{(B)} + t_n\psi_n^{(A)} + t'_{n+1}\psi_{n+1}^{(A)}, \quad (1b)$$

where  $t_n$  is the intradimer coupling and  $t'_n$  is the interdimer coupling. The infinitely periodic system exists in two configurations—a configuration  $\alpha$  where  $t_n = t_a$  and  $t'_n = t_b$ , and a configuration  $\beta$  where the values are interchanged such that  $t_n = t_b$  and  $t'_n = t_a$ . These configurations are associated with Bloch Hamiltonians

$$\mathcal{H}(k) = \begin{pmatrix} i\gamma_A & f(-k) \\ f(k) & i\gamma_B \end{pmatrix}, \quad f(k) = \begin{cases} t_a + t_b e^{ik} & (\alpha) \\ t_b + t_a e^{ik} & (\beta) \end{cases}, \quad (2)$$

delivering identical dispersion relations

$$\varepsilon_{\pm}(k) = i\bar{\gamma} \pm \sqrt{t_a^2 + t_b^2 + 2t_a t_b \cos k - \gamma^2} \quad (3)$$

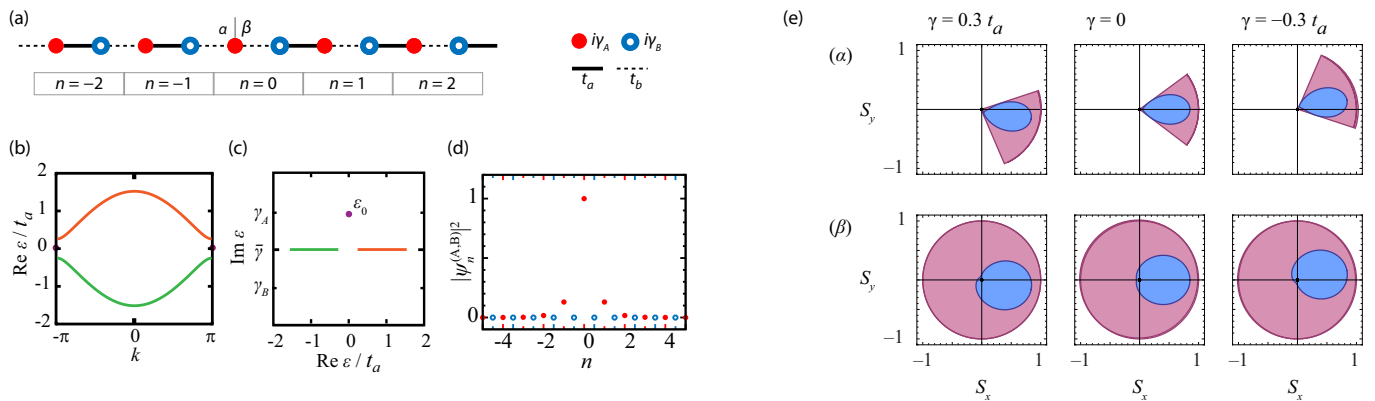


FIG. 1. (a) Complex Su-Schrieffer-Heeger (cSSH) chain with alternating couplings  $t_a$  and  $t_b$  as well as alternating imaginary onsite potential  $i\gamma_A = i(\bar{\gamma} + \gamma)$  and  $i\gamma_B = i(\bar{\gamma} - \gamma)$  (describing loss or gain in the photonic applications). For  $n < 0$  the system is in the  $\alpha$  configuration while for  $n > 0$  it is in the  $\beta$  configuration. (b) Dispersion  $\text{Re } \epsilon(k)$  of the extended states, for  $t_b = 0.6 t_a$  and  $\gamma = 0.3 t_a$ . These states have  $\text{Im } \epsilon(k) = \bar{\gamma}$ . (c) Dispersion in the complex eigenvalue plane, including the midgap state at  $\epsilon_0 = i\gamma_A$ , which forms due to the coupling defect. (d) As in the original SSH model, the midgap state is exponentially localized around the interface and is confined to the A sublattice. (e) Topological characterization of the cSSH model. The outer curve shows the trace of the pseudospin vector  $\mathbf{S}(k)$  in the  $xy$  plane, for the extended states in the upper band  $\epsilon_+(k)$  of an infinitely periodic chain in the  $\alpha$  or  $\beta$  configuration ( $t_b = 0.6 t_a$  and  $\gamma/t_a = 0.3, 0$ , or  $-0.3$ ). As in the original SSH model,  $S_z = 0$ , so that the configurations can be characterized in terms of their winding number (0 in  $\alpha$  and 1 in  $\beta$ ). The enclosed loops show the trace of the function  $g(k)$  whose position in the complex plane determines the direction of  $\mathbf{S}(k)$  according to Eq. (6). These loops encircle the origin in  $\beta$  but not in  $\alpha$ .

for extended states with dimensionless wavenumber  $k$ .

In the original SSH model with  $\bar{\gamma} = \gamma = 0$  this results in two bands, symmetrically arranged about  $\epsilon = 0$  and separated by a gap  $\Delta = 2(t_a - t_b)$ . In the cSSH model these bands are shifted into the complex plane, corresponding to decaying states if  $\text{Im } \epsilon < 0$  and amplified states if  $\text{Im } \epsilon > 0$ . However, this shift is uniform if  $|\gamma| < \gamma_c = \Delta/2$ , which is imposed henceforward. Under this condition, all extended states experience the same overall gain ( $\bar{\gamma} > 0$ ) or loss ( $\bar{\gamma} < 0$ ). In the particular case  $\bar{\gamma} = 0$  of balanced loss and gain, the dispersion remains real, which can be explained by the  $\mathcal{PT}$  symmetry  $\sigma_x[\mathcal{H}(k)]^* \sigma_x = \mathcal{H}(k)$  with Pauli matrix  $\sigma_x$  [18, 19].

The midgap state appears when the two configurations are coupled together. In Fig. 1(a), the system is in the  $\alpha$  configuration for  $n < 0$  and in the  $\beta$  configuration for  $n \geq 0$ , which results in a coupling defect in the middle of the sample. The spectrum consists of extended states within the two bands, plus an additional state at  $\epsilon_0 = i\gamma_A$ , as shown in Fig. 1(b,c). Going back to Eqs. (1), this value admits an exponentially localized solution with  $\psi_n^A = (-t_b/t_a)^{-|n|}$  and  $\psi_n^B = 0$  [Fig. 1(d)]. In the original SSH model the midgap state sits at  $\epsilon_0 = 0$  and preserves the symmetry of the spectrum. In the cSSH model the midgap state breaks this symmetry in a way that directly impacts on its amplification or decay rate—the midgap state is more stable than the extended states if  $\gamma > 0$ , and less stable if  $\gamma < 0$ . This has a topological origin, which is discussed at the end of this work. Prior to this I discuss applications of the selective amplification mechanism for the manipulation of beams and lasing.

*Beam dynamics.*—Let us first consider the manifestation of the midgap state in the beam propagation along a photonic lattice, composed of single-mode waveguides as shown in Fig. 2. Experimentally, such lattices can be realized using optical fibers, quantum wells, or femtosecond laser-writing techniques, producing in all cases arrays of waveguides with a fixed cross-sectional geometry perpendicular to the propagation direction  $z$  [20–22]. In this setting the parameters  $\gamma_A$  and  $\gamma_B$  describe the intrinsic propagation constants of the waveguides, which are lossy if  $\gamma_{A,B} < 0$  and amplifying if  $\gamma_{A,B} > 0$ . The couplings take the values  $t_a$  and  $t_b$ , depending on whether the spacing between the waveguides is  $a$  or  $b$ , respectively, and the midgap state now arises from a defect in an alternating spacing sequence. Modes with  $\text{Im } \epsilon > 0$  exponentially increase along the propagation direction  $z$  while those with  $\text{Im } \epsilon < 0$  decay.

I now set  $\gamma_A = 0$  and  $\gamma_B = -2\gamma < 0$ , corresponding a setup with passive  $A$  sites and lossy  $B$  sites. The midgap state is then lossless ( $\epsilon_0 = 0$ ) while the extended states decay uniformly according to  $\text{Im } \epsilon = \bar{\gamma} = -\gamma < 0$ . Figure 2 illustrates the beam propagation in a lattice of 101 fibers and a spacing defect in the center of the system. Panel (a) depicts the arrangement of the fibers close to the center of the sample. In panel (b), a broad wave packet is fed into the lattice with  $t_b = 0.2 t_a$ ,  $\gamma = 0.05 t_a$ . After a short transient the midgap state is populated and propagates without attenuation. In panel (c), the light is fed into a single  $A$  fiber close to the center of the sample. Again, the midgap state is populated; it is now less localized because here  $t_b = 0.6 t_a$ . In panel (d), the

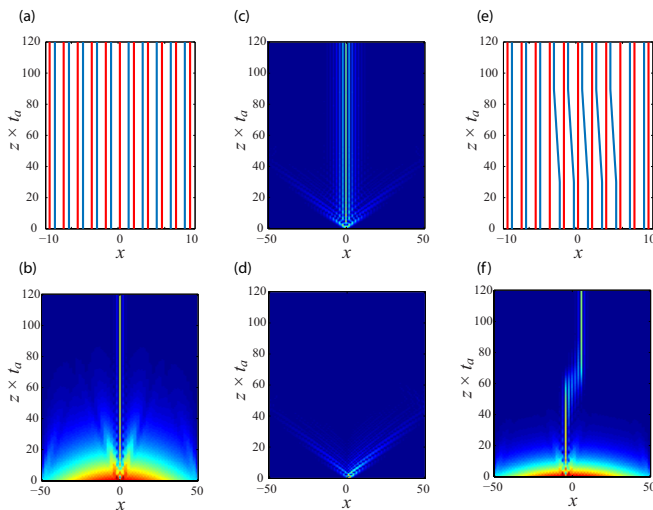


FIG. 2. (a) Realization of the cSSH model in a photonic lattice of single-mode waveguides with intrinsic propagation constants  $\gamma_A$  and  $\gamma_B$  as well as alternating spacings  $a$  and  $b$ , and a defect in that spacing sequence (around  $x = 0$ ). (b) Beam propagation of an initially broad wave packet in a lattice of 101 waveguides with  $t_b = 0.2 t_a$ ,  $\gamma_A = 0$ ,  $\gamma_B = -0.1 t_a$ . (c,d) Beam propagation with light fed into an A or B fiber close to  $x = 0$ , for a lattice with  $t_b = 0.6 t_a$ ,  $\gamma_A = 0$ ,  $\gamma_B = -0.1 t_a$ . (e) Adiabatic pumping of light: Waveguide geometry close to the center of the system. (f) Beam propagation in a lattice of 101 waveguides, with  $t_b = 0.2 t_a$ ,  $\gamma_A = 0$ ,  $\gamma_B = -0.2 t_a$ . [30]

light is fed into a neighboring B fiber of the same lattice. The beam quickly subsides as the midgap state is not populated.

Figure 2(e,f) demonstrates the feasibility of adiabatic light pumping [7, 23, 24] in a lattice where the interface gradually shifts by 5 unit cells to the right. In the transient region the couplings  $t_n$  and  $t'_n$  interpolate linearly between  $t_a$  and  $t_b$ , with  $t_b = 0.2 t_a$ ,  $\gamma = 0.1 t_a$ . Note that the shift of the beam is opposite to the shift of the interface.

These results generalize to systems with  $\gamma_A \neq 0$ . At fixed  $\gamma$ , this situation differs from the passive realization by a  $z$ -dependent intensity scaling  $\exp(2\gamma_A z)$ . In active realizations with  $\gamma_A = \bar{\gamma} + \gamma > 0 > \gamma_B = \bar{\gamma} - \gamma$ ,  $|\gamma| < \gamma_c$ , the midgap state is the only amplified state while the extended states all decay.

*Laser applications.*—When a system with active components is confined in the  $z$  direction, the midgap state serves as a selectively amplified lasing mode. Figure 3 (a) illustrates how such a system could be realized using an arrangement of amplifying and absorbing (or passive) regions separated by gaps of alternating length. This provides a topological realization of microlasing with distributed gain and loss [25–28]. While the underlying wave equation is second order in time or frequency, in standard slowly-varying envelope approximation the eigenvalues of

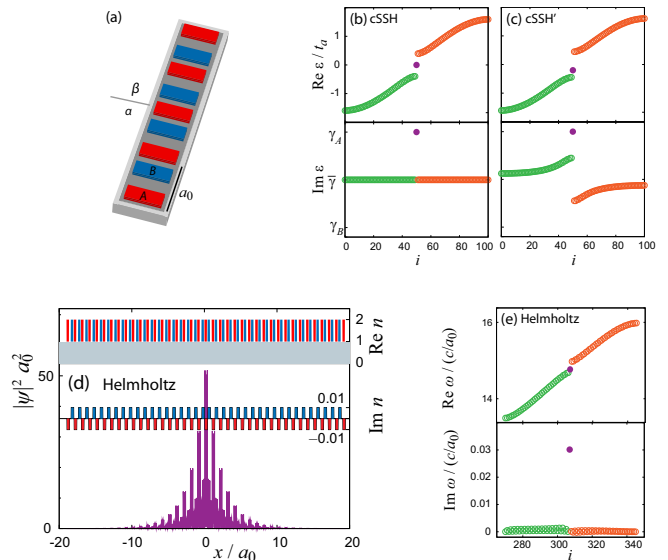


FIG. 3. (a) Realization of the cSSH model in a quasi-one-dimensional photonic laser with a staggered arrangement of active (A) and lossy (or passive) components (B) in a unit cell of size  $a_0$ . (b) Spectrum of a finite system with 101 modes ( $t_b = 0.6 t_a$ ,  $\gamma = 0.1 t_a$ ), in increasing order of  $\text{Re } \varepsilon_i$  ( $i = 0, 1, 2, \dots, 100$ ). (c) Same for complex  $\gamma = (0.1 + 0.2i) t_a$  (cSSH' model). The midgap state remains the most amplified state. (d) Implementation in a dielectric medium with regions of refractive index  $n = 1$  (passive),  $n_A = 2 - 0.01 i$  (gain) and  $n_B = 2 + 0.01 i$  (loss). Selectively amplified midgap states are predominantly localized in the gain medium. (e) The depicted midgap state (index  $i = 308$ ) is situated between bands 8 and 9 of a system of length  $40 a_0$ . [31]

the cSSH model can now be interpreted as the mode frequencies  $\omega_i = \varepsilon_i + \Omega$  around a large central frequency  $\Omega$ .

Panel (b) shows the spectrum of a finite cSSH chain with 101 lattice points. For  $\gamma > 0$  the midgap state is selectively amplified in the time domain and thus will win the mode competition. With increasing  $\bar{\gamma}$  the lasing threshold then occurs at  $\bar{\gamma} = -\gamma$ , at which point  $\gamma_A = \bar{\gamma} + \gamma = 0$  so that  $\omega_0$  crosses into the upper half of the complex plane. For  $\gamma < 0$ , on the other hand, the extended states win the mode competition and become lasing at  $\bar{\gamma} = 0$ .

Amplifying and absorbing regions with matching characteristics pose an experimental challenge. In panel (c) this is taken into account via an additional alternating real part of the onsite potential, which is equivalent to setting  $\gamma$  to a complex value (cSSH' model). This shifts the real part of the midgap state's frequency but does not affect the imaginary part, which still exceeds that of the extended states (the latter now acquire a mode dependence).

Panels (d,e) test the applicability of these predictions for an implementation of the laser in a dielectric medium with refractive index  $n_A = 2 - 0.01 i$  in the amplifying

parts and  $n_B = 2 + 0.01i$  in the absorbing parts of the system. These regions have lengths  $a_0/3$  and are separated by gaps (refractive index  $n = 1$ ) of alternating size  $a_0/12$  and  $a_0/4$ , where  $a_0$  is the length of the unit cell. The results apply to a system of length  $40 a_0$ . Midgap states form between the lowest-lying bands that approximate the continuum limit. In panels (d,e) this is illustrated for the example of bands 8 and 9; the midgap state is localized in the amplifying regions and its frequency lies much higher up in the complex plane than those of the extended states. The results correspond well to the predictions of the cSSH model, with minor deviations mostly in line with the cSSH' model.

*Topological characterization.*—Finally let us discuss how the particular features of the midgap state relate to the topological properties of the cSSH model. As in the SSH model, the difference between the  $\alpha$  and  $\beta$  configuration is captured via a topological phase associated with the Bloch functions [3, 4, 29]. To formulate this characterization it is convenient to write the eigenvectors of Hamiltonian (2) as

$$\varphi(k) = N \begin{pmatrix} f(-k) \\ \varepsilon(k) - i\gamma_A \end{pmatrix} \equiv \begin{pmatrix} \varphi^{(A)}(k) \\ \varphi^{(B)}(k) \end{pmatrix}, \quad (4)$$

where  $N$  is the normalization constant. Each extended state can then be associated with a pseudospin vector

$$\mathbf{S} = \langle (\sigma_x, \sigma_y, \sigma_z) \rangle = (S_x, S_y, S_z). \quad (5)$$

In the SSH model,  $|\varphi_A|^2 = |\varphi_B|^2$ , thus  $S_z = 0$  so that  $\mathbf{S}$  is confined to the  $xy$ -plane. Remarkably, as long as  $|\gamma| < \gamma_c$  this property remains preserved in the cSSH model, for any value of  $\bar{\gamma}$ . From the expression given above, the direction of the pseudospin can be read off from

$$S_x + iS_y \propto (\varepsilon(k) - i\gamma_A)f(k) \equiv g(k). \quad (6)$$

Figure 1(e) uses this relation to trace out the pseudospin as  $k$  passes through the Brillouin zone ( $-\pi < k < \pi$ , shown for the upper band  $\varepsilon_+(k)$ ). In the  $\alpha$  configuration, the function  $g(k)$  (enclosed loop) does not encircle the origin of the complex plane; the pseudospin therefore librates and traces out an arc (winding number 0, topological phase 0). In the  $\beta$  configuration  $g(k)$  encircles the origin; the pseudospin therefore rotates and traces out a circle (winding number 1, topological phase  $\pi$ ).

This topological robustness is further illuminated by considering the chiral symmetry  $\sigma_z H^* \sigma_z = -H$ , where  $\sigma_z$  acts in the AB subspace. One can verify directly from Eq. (1) that this symmetry persists in the cSSH model. For the pure configurations,  $\sigma_z [\mathcal{H}(-k)]^* \sigma_z = -\mathcal{H}(k)$ , which implies particle-hole symmetry of the dispersion, while in the presence of the defect the chiral symmetry guarantees the existence of a midgap state [29]. Due to the localization on the  $A$  sublattice, this state possesses a fully polarized pseudospin  $\mathbf{S} = (0, 0, 1)$  and inherits

the complex potential on this sublattice, which thus determines its eigenvalue  $\varepsilon_0 = i\gamma_A = i\bar{\gamma} + i\gamma$ . Notably, this is still consistent with the constraint  $\varepsilon_0 = -\varepsilon_0^*$  implied by chirality; the specific value  $\varepsilon_0 = 0$  only follows in the hermitian limit of the SSH model. The extended states populate both sublattices equally, which results in  $\text{Im} \varepsilon(k) = i\bar{\gamma}$ . Therefore, the midgap state is more stable than the extended states if  $\gamma > 0$ , and less stable if  $\gamma < 0$ .

*Conclusions.*— In conclusion, photonic systems can exhibit exponentially localized, topologically protected midgap states whose stability may be controlled via distributed loss and gain. Such states can be induced in beam propagation through photonic lattices, where they provide a platform for adiabatic pumping of light, and in photonic crystal lasers with inhomogeneous gain, where they exhibit selective level amplification. Remarkably, the midgap states maintain their topological protection even though the loss and gain renders the underlying Hamiltonian nonhermitian and breaks the time reversal symmetry of the system. This demonstrates the utility of topological concepts in genuinely photonic settings.

- 
- [1] E. Yablonovitch, Phys. Rev. Lett. **58**, 2059 (1987).
  - [2] S. John, Phys. Rev. Lett. **58**, 2486 (1987).
  - [3] M. Z. Hasan and C. L. Kane, Rev. Mod. Phys. **82**, 3045 (2010).
  - [4] X. L. Qi and S. C. Zhang, Rev. Mod. Phys. **83**, 1057 (2011). *Rev. Mod. Phys.* **83**, 1057 (2011).
  - [5] Z. Wang, Y. Chong, J. D. Joannopoulos, and M. Soljačić, Nature **461**, 772 (2009).
  - [6] M. Hafezi, E. A. Demler, M. D. Lukin, and J. M. Taylor, Nature Phys. **7**, 907 (2011).
  - [7] Y. E. Kraus, Y. Lahini, Z. Ringel, M. Verbin, and O. Zilberberg, Phys. Rev. Lett. **109**, 106402 (2012).
  - [8] H. Schomerus and N. Yunger Halpern, Phys. Rev. Lett. **110**, 013903 (2013).
  - [9] M. C. Rechtsman, J. M. Zeuner, A. Tünnermann, S. Nolte, M. Segev, and A. Szameit, Nature Photonics, published online, doi:10.1038/nphoton.2012.302.
  - [10] K. Fang, Z. Yu, and S. Fan, Nature Photonics **6**, 782 (2012).
  - [11] T. Kitagawa, M. A. Broome, A. Fedrizzi, M. S. Rudner, E. Berg, I. Kassal, A. Aspuru-Guzik, E. Demler, and A. G. White, Nature Communications **3**, 882 (2012).
  - [12] X.-L. Qi, T. L. Hughes, and S.-C. Zhang, Phys. Rev. B **78**, 195424 (2008).
  - [13] S. Ryu, A. P. Schnyder, A. Furusaki, and A. W. W. Ludwig, New J. Phys. **12**, 065010 (2010).
  - [14] W. P. Su, J. R. Schrieffer, and A. J. Heeger, Phys. Rev. Lett. **42**, 1698 (1979).
  - [15] K. G. Makris, R. El-Ganainy, D. N. Christodoulides, and Z. H. Musslimani, Phys. Rev. Lett. **100**, 103904 (2008).
  - [16] A. Guo, G. J. Salamo, D. Duchesne, R. Morandotti, M. Volatier-Ravat, V. Aimez, G. A. Siviloglou, and D. N. Christodoulides, Phys. Rev. Lett. **103**, 093902 (2009).
  - [17] C. E. Rüter, K. G. Makris, R. El-Ganainy, D. N. Christodoulides, M. Segev, and D. Kip, Nature Phys.

- 6**, 192 (2010).
- [18] M. C. Zheng, D. N. Christodoulides, R. Fleischmann, and T. Kottos, *Phys. Rev. A* **82**, 010103 (2010).
- [19] H. Ramezani, D. N. Christodoulides, V. Kovanic, I. Vitebskiy, and T. Kottos, *Phys. Rev. Lett.* **109**, 033902 (2012).
- [20] D. N. Christodoulides, F. Lederer, and Y. Silberberg, *Nature (London)* **424**, 817 (2003).
- [21] A. Szameit, D. Blömer, J. Burghoff, T. Schreiber, T. Pertsch, S. Nolte, A. Tünnermann, and F. Lederer, *Opt. Express* **13**, 10 552 (2005).
- [22] Y. Lahini, R. Pugatch, F. Pozzi, M. Sorel, R. Morandotti, N. Davidson, and Y. Silberberg, *Phys. Rev. Lett.* **103**, 013901 (2009).
- [23] Y. Lahini, F. Pozzi, M. Sorel, R. Morandotti, D. N. Christodoulides, and Y. Silberberg, *Phys. Rev. Lett.* **101**, 193901 (2008).
- [24] A. Salandrino, K. Makris, D. N. Christodoulides, Y. Lahini, Y. Silberberg, and R. Morandotti, *Optics Communications* **282** 4524 (2009).
- [25] J. Andreasen and H. Cao, *Opt. Lett.* **34**, 3586 (2009).
- [26] H. Schomerus, *Phys. Rev. Lett.* **104**, 233601 (2010).
- [27] S. Longhi, *Phys. Rev. A* **82**, 031801(R) (2010).
- [28] Y. D. Chong, L. Ge, and A. D. Stone, *Phys. Rev. Lett.* **106**, 093902 (2011).
- [29] S. Ryu and Y. Hatsugai, *Phys. Rev. Lett.* **89**, 077002 (2002).
- [30] The beam dynamics in the photonic lattices of Fig. 2 is obtained in coupled-mode theory [20–22]. I denote by

$\Psi_n^{(A,B)}(z)$  the amplitudes of the modes in the  $n$ th unit cell. The evanescent coupling between the two waveguides within the  $n$ th unit cell is again denoted as  $t_n$ , while the coupling between neighbouring waveguides in the cell  $n-1$  and  $n$ th is denoted as  $t'_n$ . The couplings take the values  $t_a$  and  $t_b$ , depending on whether the spacing between the waveguides is  $a$  or  $b$ , respectively, and the midgap state now arises from a defect in an alternating spacing sequence. In this setting the parameters  $\gamma_A$  and  $\gamma_B$  describe the intrinsic propagation constants of the waveguides, which are lossy if  $\gamma_{A,B} < 0$  and amplifying if  $\gamma_{A,B} > 0$ . The propagation of monochromatic waves along  $z$  is then described by the coupled-mode equations

$$i(\partial_z - \gamma_A)\Psi_n^{(A)} = t'_n\Psi_{n-1}^{(B)} + t_n\Psi_n^{(B)}, \quad (7a)$$

$$i(\partial_z - \gamma_B)\Psi_n^{(B)} = t_n\Psi_n^{(A)} + t'_{n+1}\Psi_{n+1}^{(A)}. \quad (7b)$$

For systems that are homogeneous in  $z$ , the eigenmodes are obtained by the separation  $\Psi_n^{(A,B)}(z) = \exp(-i\varepsilon z)\psi_n^{(A,B)}$ , where  $\varepsilon$  and  $\psi_n^{(A,B)}$  are determined by the tight-binding model (1). The results in Fig. 2 follow by numerical integration of Eq. (7) with the Crank-Nicholson method.

- [31] The results for the quasi-one-dimensional laser in Fig. 3 have been obtained by numerically solving the one-dimensional Helmholtz equation  $(\partial_x^2 + n^2(x)\omega^2/c^2)\psi(x) = 0$  for a system of length  $40a_0$ , with space discretized in steps  $a_0/60$ .